Optical Materials 51 (2016) 185–189

Contents lists available at ScienceDirect

Optical Materials

journal homepage: www.elsevier.com/locate/optmat

Optical ridge waveguides in Er^{3+}/Yb^{3+} co-doped phosphate glass produced by ion irradiation combined with femtosecond laser ablation for guided-wave green and red upconversion emissions

Chen Chen [a], Ruiyun He [a], Yang Tan [a], Biao Wang [b], Shavkat Akhmadaliev [c], Shengqiang Zhou [c], Javier R. Vázquez de Aldana [d], Lili Hu [b], Feng Chen [a,*]

[a] School of Physics, State Key Laboratory of Crystal Materials and Key Laboratory of Particle Physics and Particle Irradiation (Ministry of Education), Shandong University, Jinan 250100, China
[b] Shanghai Institute of Optics and Fine Mechanics, Chinese Academy of Sciences, China
[c] Institute of Ion Beam Physics and Materials Research, Helmholtz-Zentrum Dresden-Rossendorf, Dresden 01314, Germany
[d] Laser Microprocessing Group, Universidad de Salamanca, Salamanca 37008, Spain

ARTICLE INFO

Article history:
Received 16 September 2015
Received in revised form 25 October 2015
Accepted 25 November 2015
Available online 30 November 2015

Keywords:
Ridge optical waveguides
Er^{3+}/Yb^{3+} co-doped phosphate glass waveguides
Upconversion
Laser ablation
Ion irradiation

ABSTRACT

This work reports on the fabrication of ridge waveguides in Er^{3+}/Yb^{3+} co-doped phosphate glass by the combination of femtosecond laser ablation and following swift carbon ion irradiation. The guiding properties of waveguides have been investigated at 633 and 1064 nm through end face coupling arrangement. The refractive index profile on the cross section of the waveguide has been constructed. The propagation losses can be reduced considerably after annealing treatment. Under the optical pump laser at 980 nm, the upconversion emission of both green and red fluorescence has been realized through the ridge waveguide structures.

1. Introduction

The optical materials doped with erbium ions (Er^{3+}) have attracted much attention owing to their promising applications such as laser generation and signal amplification [1–3]. Besides, the multiple energy level system of erbium ion also provides the possibility for upconversion emission. The upconversion is an anti-Stokes process in which the sequential absorption of two or more photons leads to the emission of light at shorter wavelength than the excitation wavelength. At present, there is great interest in luminescent materials for efficient upconversion from near infrared to visible radiation, which is useful for high-capacity data storage optical devices [4–6]. The phosphate glass composed of P_2O_5, Al_2O_3, MgO, etc. has been proved to be an ideal host family for the doping of erbium ions with high concentration [7,8].

As one of the basic components in integrated optics, optical waveguide is able to localize the propagation of light field within the space at micron scale, thus increase the light density considerably with respect to that in the bulk material [9,10]. The fabrication of waveguides has been implemented in a large number of optical materials by different techniques, such as thermal ion indiffusion [11], ion exchange [12], thin film deposition [13], ion implantation/irradiation [14], and ultrafast laser inscription [15].

Swift heavy ion irradiation, as an alternative solution of traditional ion implantation, has been universally applied to produce planar waveguides due to its controllable modification of refractive index at tunable depth beneath the material surface [16]. In addition, compared with planar waveguide, the ridge waveguide is superior for its two-dimensional (2D) confinement of the light propagation at the transverse sections. To construct 2D ridge waveguides, swift heavy ion irradiation or ion implantation must be combined with other technique, such as wet or dry etching [17], diamond blade dicing [18], and laser ablation, to remove certain parts of the planar waveguides in order to achieve refractive index contrast along the horizontal direction for light field confinement. The combination of laser ablation and swift heavy ion irradiation has been implemented in several materials to manufacture ridges with high quality [19,20]. As for upconversion emission in waveguide, Liu et al. have reported on the green upconversion

* Corresponding author.
E-mail address: drfchen@sdu.edu.cn (F. Chen).

http://dx.doi.org/10.1016/j.optmat.2015.11.042
0925-3467/

pumped by 800-nm laser in planar waveguide based on Er^{3+}/MgO codoped $LiNbO_3$ crystal [21]. Moreover, Liu et al. have realized white upconversion luminescence in $Tm^{3+}/Ho^{3+}/Yb^{3+}$ triply doped K^+–Na^+ ion-exchanged aluminum germanate glass channel waveguide [22].

In this work, we report, the first time to our knowledge, on the fabrication of ridge waveguides via the combination of laser ablation and swift heavy ion irradiation in an Er^{3+}/Yb^{3+} co-doped phosphate glass. The waveguide properties were investigated by using end-face coupling method. With the excitation of 980 nm continuous-wave (CW) laser, both green and red upconversion emissions have been realized inside ridge waveguide structure.

2. Experiments in details

The Er^{3+}/Yb^{3+} co-doped phosphate glass with 1.5 wt.% Er_2O_3 and 4.5 wt.% Yb_2O_3 was manufactured by Shanghai Institute of Optics and Fine Mechanics, Chinese Academy of Sciences, China. It was cut into a wafer with dimension of $10 \times 10 \times 2$ mm^3. Its surface (10×10 mm^2) and two parallel end faces (10×2 mm^2) were optically polished. In order to produce ridge structure, we applied the technique of femtosecond laser ablation. A Ti:Sapphire laser system, which delivered 120 fs pulses, linearly polarized at 796 nm and with a repletion rate of 1 kHz, was used to microstructure the ridge structures. The laser beam was focused by a 20× microscope objective (N.A. = 0.6) and with the energy of 2.1 μJ. With the repeated scans of the femtosecond laser beam at the velocity of 50 μm/s, several parallel ablated grooves with depth of ~20 μm have been formed, which separate the sample into a few independent ridge shaped regions. The intervals between two neighbor grooves (the widths of ridges), were set to be 15, 20, 25, 30 and 35 μm respectively (seeing Fig. 1(c)). Then we fabricated waveguide layer through the process of swift heavy ion irradiation. The C^{5+} ions accelerated to 15 MeV, through a 3MV tandem accelerator at Helmholtz-Zentrum Dresden-Rossendorf, struck the sample surface at the fluence of 4×10^{14} ions/cm^2, as shown in Fig. 1(b). During this process, ion beam current density remained at a low level (~10 nA/cm^2) to avoid the heating and charging of the sample.

For further characterization of more details, we measured the ridges waveguides with certain sizes by a microscope. To investigate the mode distributions in the waveguides, we utilized the end face coupling method. Fig. 2 depicts the experimental arrangement. A 633-nm He–Ne laser and a 1064 nm CW solid-state laser were selected as laser sources, respectively. The half-wave plates corresponding to different wavelength served as polarizer to produce vertically polarized light field (TM mode) and horizontal polarized one (TE mode). The polarized input beam was focused by the first microscope objective and coupled into waveguide structure. The second microscope objective was used to collect the output light from the ridge waveguides. A CCD camera or a power meter was used to image the waveguide modes and measure the light powers for loss evaluation, respectively.

As for the experiment of upconversion emission, the equipment was basically similar to that of end-face coupling in principle. However, the microscope objectives used in end-face coupling experiments were replaced by two convex lenses and the laser source was changed to a 980 nm CW diode laser for providing the excitation of the energy level transition of Er^{3+} and Yb^{3+} ions inside the waveguides. The upconversion fluorescence signals emitted from the sample were finally received by a fluorescence spectrometer at the end of light path.

3. Results and discussion

Fig. 3 exhibits microscopic photographs in the cross sections and guiding mode profiles of ridges with different widths at the wavelength of 633 and 1064 nm. From these microscopic photographs, the ridge outlines can be seen clearly. The depth of ablated grooves is measured to be ~20 μm, and the thickness of waveguide layer formed by swift carbon ion irradiation is ~11 μm. In terms of mode profiles, we find that, in vertical direction, only one mode could be supported; while in horizontal direction, the multiple modes only exist in the ridges with width over 30 μm. For TE and TM polarization, the guiding modes are extremely close to each other in the entire shape and the distribution of light intensity, suggesting the isotropic feature of phosphate glass. According to these results, we conclude that such ridge waveguides are able to supply remarkable confinement of light propagation vertically and horizontally, applicable in visible (633 nm) and near infrared wavelengths (1064 nm).

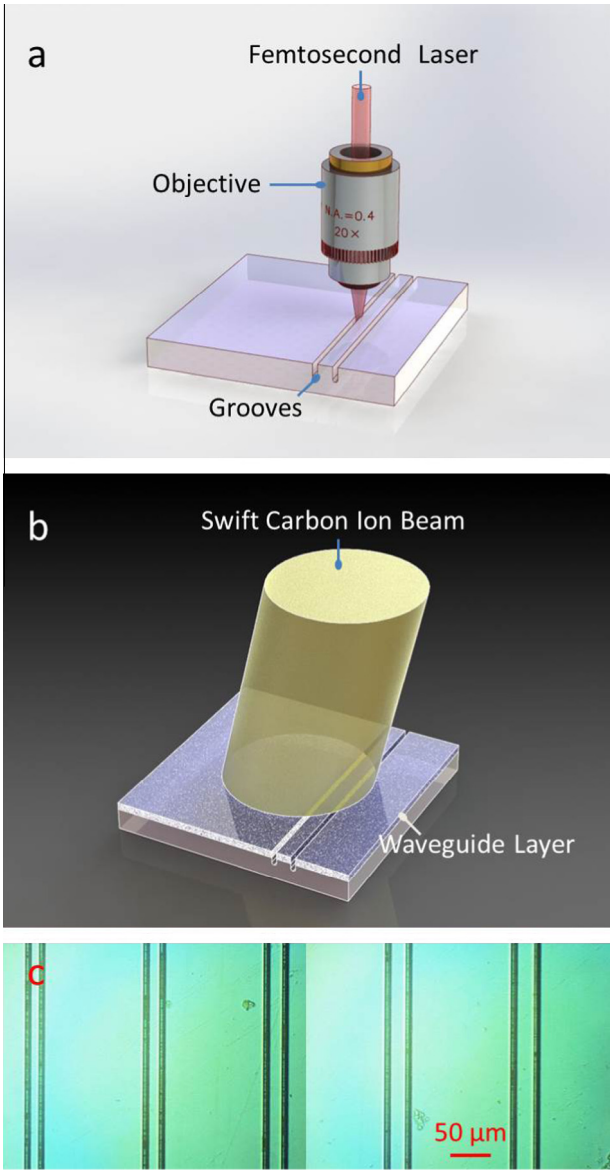

Fig. 1. The schematic plots of ridge waveguides fabrication processes: (a) femtosecond laser ablation, (b) swift carbon ion irradiation, with the microscopic image from the sample surface (c).

We have simulated the energy deposition of carbon ions happened in the irradiation process using code Stopping and Range of Ions in Matter 2013 (SRIM 2013) [23]. As shown in Fig. 4(a), the stopping power curves reveal the major factor of the interaction between incident ion and target sample, which is the elec-

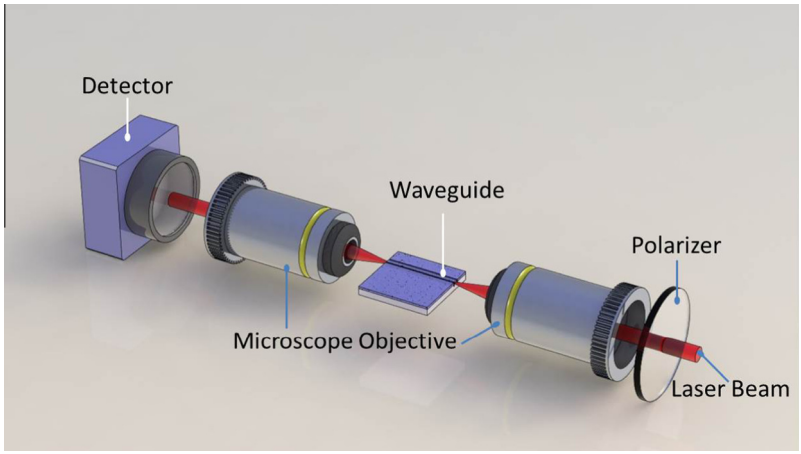

Fig. 2. The schematic plot of end-face coupling arrangement.

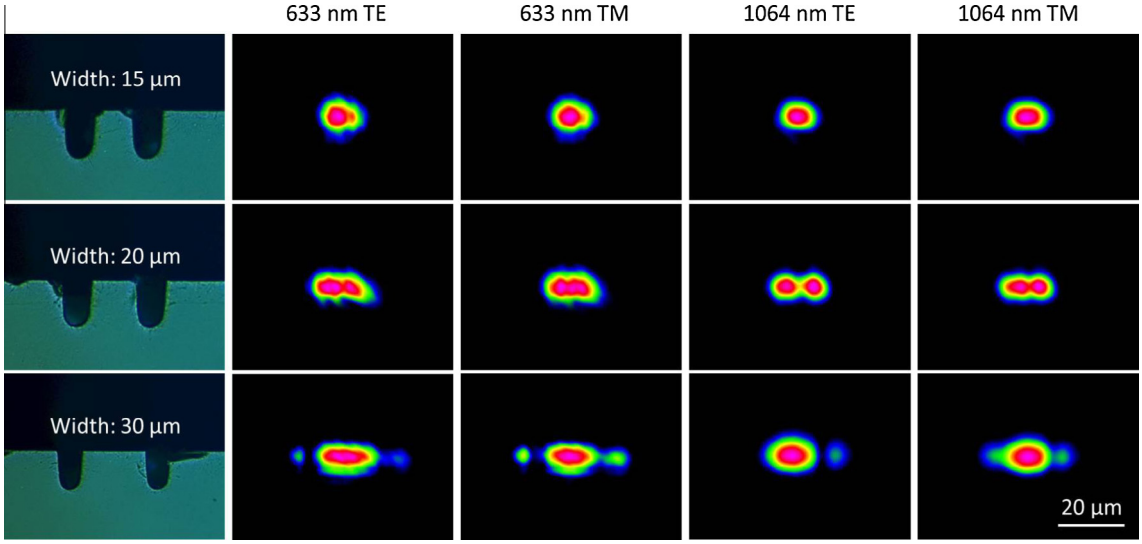

Fig. 3. The microscopic photographs for ridge structures at the cross section (left column), and measured modal distributions of Er, Yb:phosphate ridge waveguides (other columns). The scale bar is valid for all figures.

tronic damage. The electronic stopping power (S_e) climbs slowly from the surface of the sample, gets the maximum at the depth around 8 μm, and then falls rapidly. It declines into zero at the depth of ~11 μm, which is exactly the depth of waveguide layer measured under microscope. The nuclear stopping power (S_n) is much lower, compared with the S_e. Also according to the previous works on swift heavy ion irradiation on other materials [24], it seems reasonable to conclude that the electronic energy deposition induced damage of original matrix plays the more critical role in the formation of the refractive index changed layer. Based on the results shown above, we have reconstructed the distribution of the refractive index in the waveguide region. As depicted in Fig. 4(b), the index varies smoothly from the value of 1.550–1.555. The largest index change occurs at the position where the S_e reaches the top (~8 μm beneath the surface). In the region near surface or at the end of ions' incident range, the index remains 1.550, the refractive index of substrate. The maximum contrast of the refractive index Δn (~0.005) was calculated by the equation [25]:

$$\Delta n = \frac{\sin^2 \Theta_m}{2n} \quad (1)$$

where n stands for the refractive index of substrate, and Θ_m symbolize the maximum incident angle, which is the largest angel allowed between the incident beam and the end face normal. The reasonability of this reconstructed refractive index profile has been tested through importing it into the Software Rsoft Beam PROP 8.0© [26]. Based on such index profile, the software simulated the light field propagation to obtain the mode distribution by performing the Finite Difference Beam Propagation Method (FD-BPM) [27]. Fig. 4(c) displays the simulated mode profile inside the ridge of 15 μm wide, polarized along TM direction at 633 nm, which is fundamentally similar to the measured one (see Fig. 3). Discarding the different background colors and picture scales, these two profiles have more features in common such as the shape of light spot and the distribution of light intensity. The comparison demonstrates that the real refractive index within the waveguide layer can be faithfully reflected by the reconstructed profile. For a more intuitive look, the three-dimensional modal distribution is also given in Fig. 4(d).

The propagation losses of waveguides at TM polarization measured by end face coupling method are listed in Table 1, with the error of 0.1 dB/cm. As a consequence of the isotropic character in bulk material, the waveguide losses along TE polarization have

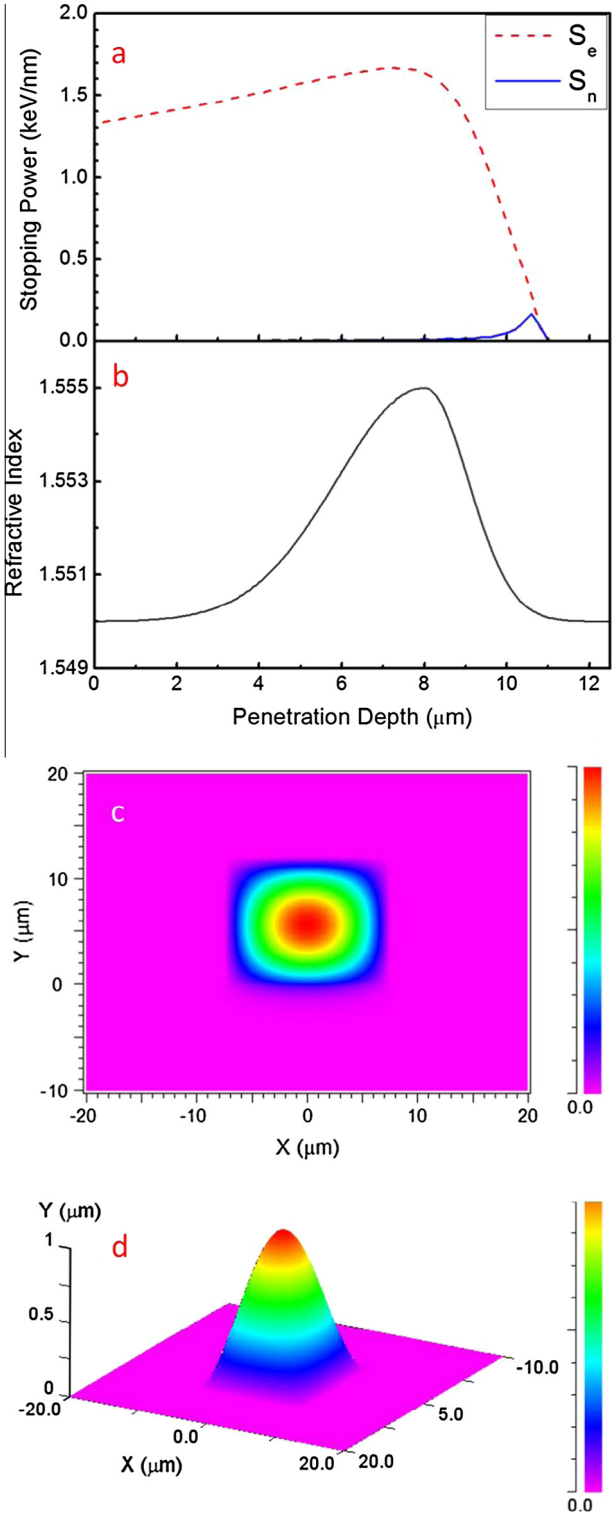

Fig. 4. (a) The electronic (S_e) and nuclear (S_n) stopping powers as functions of waveguide depth; (b) the reconstructed profile of refractive index versus waveguide depth; (c) and (d), simulated 2D and 3D modal distributions of Er, Yb: phosphate ridge.

almost the same values with TM ones considering the range of error. From the table, one can get the knowledge that as the width of ridge gets smaller, the loss value become larger. For instance, at the wavelength of 633 nm, the propagation loss of 35 um wide ridge is measured to be ~2.1 dB/cm, while the loss of 15 um one

Table 1
The propagation losses of Er, Yb:phosphate ridge waveguides.

Ridge width (μm)	Loss at 633 nm (dB/cm)		Loss at 1064 nm (dB/cm)	
	Before annealing	After annealing	Before annealing	After annealing
15	5.1	4.1	5.6	4.4
20	4.0	3.2	4.6	3.9
25	2.9	2.2	4.2	3.3
30	2.7	2.0	4.0	3.1
35	2.1	1.8	3.6	2.9

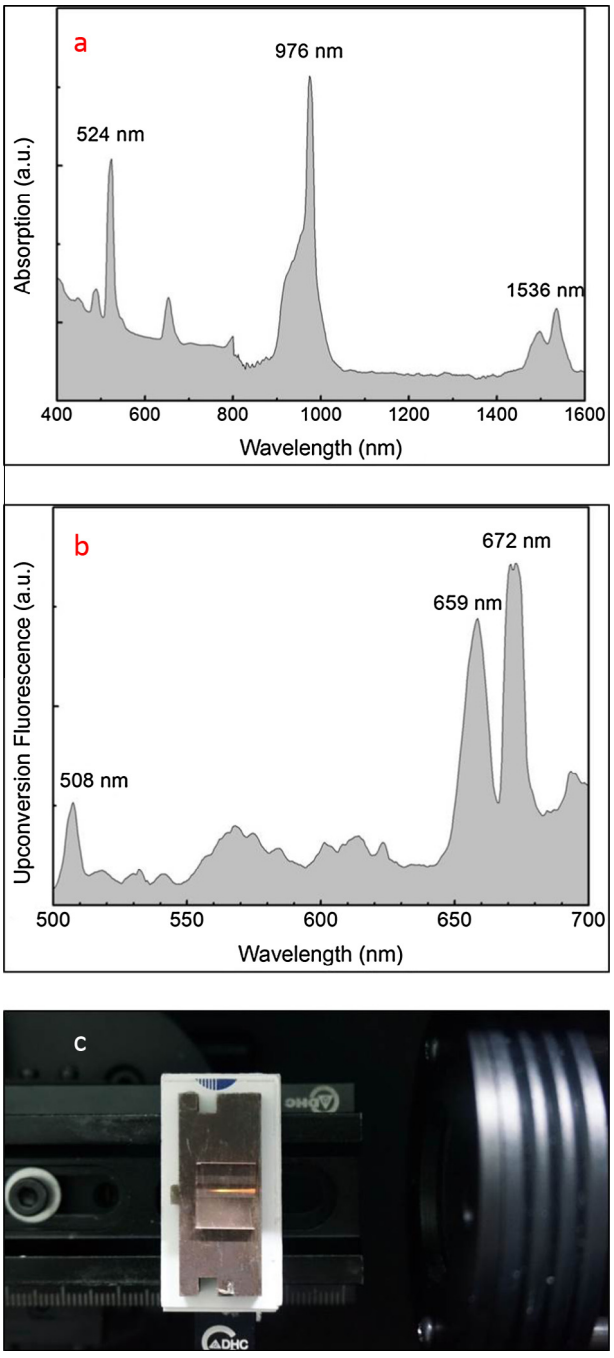

Fig. 5. Absorption (a) and upconversion (b) spectra of Er, Yb:phosphate ridge waveguide, with the photograph of upconversion fluorescence (c).

is up to ~5.1 dB/cm. Comparing the loss values at different wavelength within the same guide, we find that the loss at 1064 nm is slightly higher than that at 633 nm, which seems to be reasonable because of the more tight confinement of light at shorter wavelength. The annealing treatment took place in a tubular oven at the temperature of 200 °C for 1 h, after which the loss measurement was repeated. The data have proved the notable effect of annealing treatment in loss reducing, as the loss of 25 μm waveguide was decreased from ~4.2 dB/cm to ~3.3 dB/cm at 1064 nm, so did other cases.

The absorption spectrum of the sample was measured with a spectrophotometer in the range from 200 to 2000 nm, as presented in Fig. 5(a). The spectrum contains three main peaks centered at 524, 976 and 1536 nm respectively. Among them the absorption near 980 nm was the most intensive one with the largest bandwidth, thus we chose 980-nm-laser as the pump source.

As for upconversion fluorescence emission in the ridge waveguide, the spectrum was collected in the range from 500 to 700 nm, as shown in Fig. 5(b). It consists of two basic parts: the green upconversion peaked at 508 nm, along with the red upconversion peaked at 659 and 672 nm. For green upconversion, the Yb^{3+} ions were excited to state $^2F_{5/2}$ from $^2F_{7/2}$ under 980 nm pump laser. Meanwhile, the Er^{3+} ion was pumped from the ground state $^4I_{15/2}$ to the excited state $^4I_{11/2}$ temporarily by absorbing a photon at 980 nm or obtaining the energy from Yb^{3+} ion, and promoted to the level of $^4F_{7/2}$ through another photon absorption or energy transfer. Afterwards, the Er^{3+} ion returned to the ground state $^4I_{15/2}$ straight with the emission of a photon oscillated at around 508 nm. The red upconversion was chiefly originated from the transition from $^4F_{9/2}$ to the ground state $^4I_{15/2}$. The state of $^4F_{9/2}$ could be populated through two possible mechanisms. One is the nonradiative relaxation from the upper state $^4F_{7/2}$, while the other is the direct transition from the state $^4I_{13/2}$, which could be relaxed nonradiatively from $^4I_{11/2}$. Moreover, as the photograph presents in Fig. 5(c), the color of upconversion luminescence is a mixture of green and red, in great accordance with the information delivered from emission spectrum.

4. Conclusion

Ridge waveguides were manufactured in Er^{3+}/Yb^{3+} co-doped phosphate glass by femtosecond laser ablation along with swift carbon ion irradiation. The modal profiles and propagation losses were measured under 633 and 1064 nm, respectively. A refractive index profile was reconstructed based on the simulation of ion irradiation. With optical excitation at 980 nm, the upconversion emission of both green and red fluorescence was found within the ridges.

Acknowledgements

This work was supported by the National Natural Science Foundation of China (No. 11305094). S.Z. acknowledges the funding by the Helmholtz-Gemeinschaft Deutscher Forschungszentren (HGF-VH-NG-713). J.R. Vázquez de Aldana thanks the support from Junta de Castilla y León (Project SA086A12-2).

References

[1] P. Tang, J. Liu, B. Huang, C. Xu, C. Zhao, S. Wen, Opt. Express 23 (2015) 11037–11042.
[2] S. Jain, N.K. Thipparapu, P. Barua, J.K. Sahu, IEEE Photon. Technol. Lett. 27 (2015) 356–358.
[3] J. Hoyo, V. Berdejo, T. Toney Fernandez, A. Ferrer, A. Ruiz, J.A. Valles, M.A. Rebolledo, I. Ortega-Feliu, J. Solis, Laser Phys. Lett. 10 (2013) 105802.
[4] D.M. Wu, A. García-Etxarri, A. Salleo, J.A. Dionne, J. Phys. Chem. Lett. (2014) 4020–4031.
[5] Z. Chen, H. Jia, X. Zhang, J. Liu, S. Zeng, Y. Li, Z. Ma, G. Dong, J. Qiu, J. Am. Ceram. Soc. 98 (2015) 2508–2513.
[6] B. Joshi, Y.K. Kshetri, R. Adhikari, S.W. Lee, Ceram. Int. 41 (2015) 6455–6462.
[7] B.I. Denker, B.I. Galagan, V.A. Kamynin, A.S. Kurkov, Y.E. Sadovnikova, S.L. Semenov, S.E. Sverchkov, V.V. Velmiskin, E.M. Dianov, Laser Phys. Lett. 10 (2013) 055109.
[8] K.H. Mahmoud, Z.M. El-Bahy, A.I. Hanafy, J. Non-Cryst. Solids 363 (2013) 116–120.
[9] E.J. Murphy, Integrated Optical Circuits and Components: Design and Applications, Marcel Dekker, New York, 1999.
[10] G. Lifante, Integrated Photonics: Fundamentals, Wiley, Atrium, 2008.
[11] T.G. Giallorenzi, E.J. West, R. Kirk, R. Ginther, R.A. Andrews, Appl. Opt. 12 (1973) 1240–1245.
[12] B.J. Chen, L.F. Shen, E.Y.B. Pun, H. Lin, Opt. Mater. Express 5 (2015) 113–123.
[13] S. Ohya, B. Chiaro, A. Megrant, C. Neill, R. Barends, Y. Chen, J. Kelly, D. Low, J. Mutus, P.J.J. O'Malley, P. Roushan, D. Sank, A. Vainsencher, J. Wenner, T.C. White, Y. Yin, B.D. Schultz, C.J. Palmstrom, B.A. Mazin, A.N. Cleland, J.M. Martinis, Supercond. Sci. Technol. 27 (2014) 015009.
[14] I. Banyasz, S. Berneschi, M. Bettinelli, M. Brenci, M. Fried, N.Q. Khanh, T. Lohner, G.N. Conti, S. Pelli, P. Petrik, G.C. Righini, A. Speghini, A. Watterich, Z. Zolnai, IEEE Photonics J. 4 (2012) 721–727.
[15] Y. Duan, P. Dekker, M. Ams, G. Palmer, M.J. Withford, Opt. Mater. Express 5 (2015) 416–422.
[16] F. Chen, X. Wang, K. Wang, Opt. Mater. 29 (2007) 1523–1542.
[17] K. Furuya, K. Nakanishi, R. Takei, E. Omoda, M. Suzuki, M. Okano, T. Kamei, M. Mori, Y. Sakakibara, Appl. Phys. Lett. 100 (2012) 251108.
[18] C. Chen, Q. Luan, R. He, C. Cheng, S. Akhmadaliev, S. Zhou, H. Yu, H. Zhang, F. Chen, Opt. Laser Technol. 68 (2015) 84–88.
[19] Y. Jia, Y. Tan, C. Cheng, J.R. Vázquez de Aldana, F. Chen, Opt. Express 22 (2014) 12900–12908.
[20] Q. Luan, Y. Jia, Y. Wang, S. Akhmadaliev, S. Zhou, J.R. Vázquez de Aldana, Y. Tan, F. Chen, Opt. Mater. Express 4 (2014) 1166–1171.
[21] H. Liu, Y. Jia, Y. Ren, S. Akhmadaliev, S. Zhou, F. Chen, Nucl. Instrum. Methods B 320 (2014) 22–25.
[22] X. Liu, B. Chen, E.Y.B. Pun, H. Lin, Opt. Mater. 35 (2013) 590–595.
[23] J.F. Ziegler, Computer Code. <http://www.srim.org>.
[24] F. Chen, Laser Photon. Rev. 6 (2012) 622–640.
[25] J. Siebenmorgen, T. Calmano, K. Petermann, G. Huber, Opt. Express 18 (2010) 16035–16040.
[26] Rsoft Design Group, Computer software BeamPROP version 8.0. <http://www.rsoftdesign.com>.
[27] D. Yevick, W. Bardyszewiski, Opt. Lett. 17 (1992) 329.